

Validation and Verification of CFD Prediction of Fluid Flow of a Submerged Vertical Round Jet

Nurul Hasan¹, Ahmed Oliur Rahman² and Md. Shah Alam³



Received: 27 May 2018
Accepted: 08 June 2018
Published: 30 June 2018
Publisher: Deer Hill Publications
© 2018 The Author(s)
Creative Commons: CC BY 4.0

ABSTRACT

Verification and validation are the main two vital items to consider a CFD simulation project. In the proposed research article these steps are applied for a vertical round submerged jet into a cylindrical bath. An axisymmetric domain minimized the computational cost as the Navier-Stokes equation is simplified and a finite volume method (FVM) is used to solve continuity and momentum equation using commercial computational fluid dynamics, CFD (Fluent) software. Verification refers to solving equation right, and a step-by-step grid independence tests were performed. For validation, experimental data was produced under the same ARC funding using laser Doppler velocimetry (LDV). Among the turbulence model, *SST* was found to predict the flow behavior better than *k-ε* realization or *RSM* models.

Keywords: Turbulent flow, submerged jet, validation of CFD, verification of CFD

LIST OF SYMBOL/ABBREVIATION

Re_j	Jet Reynolds no
D_c	Cylinder diameter (m)
H_c	Cylinder height (m)
d_0	Jet diameter (m)
h	Water level (m)
<i>RSM</i>	Reynold Stress Model

1 INTRODUCTION

Numerous papers are published without a strategic verification and without coordinating with the experimentalists. So in many cases the mesh in CFD is not optimized. On the other hand, the published experimental data are not well-analyzed or well-presented. The boundary conditions for the CFD do not always represent the total physics. There are difficulties for any experimental data to produce; not the same way there are problems in all the turbulence models of CFD.

A receiving bath when receives a submerged jet [1,2], the fluid decelerates and spreads, and this process continues as it entrains the surrounded liquid. To uniform the turbulence intensity and effect on the receiving bath, a honeycomb [3] can be used. This might also suppress a possible swirl [4] which can be ignored for practical purpose. The CFD [5-7] investigations performed previously in this area were without any proper verification of the solution, the computational Central Line velocity can be plotted against the experimental data at the same location. One of

N. Hasan¹ ✉, A. O. Rahman² and M. S. Alam³

¹Petroleum and Chemical Engineering Programme, Faculty of Engineering
Universiti Teknologi Brunei, Jalan Tungku Link, Gadong BE 1410, Brunei Darussalam
E-mail: nurulhasan@asme.org

²Faculty of Engineering, Deakin University, Geelong, Victoria 3220, Australia
E-mail: aorahman@deakin.edu.au

³Department of Civil Engineering, University of Bahrain, PO Box 32038, Sakheer, Kingdom of Bahrain
E-mail: malam@uob.edu.bh

the best set of data is available from Bayly et al. [8]. Without verification, previous authors have performed an investigation, e.g., a mesh of 54X44 [8] is not enough as shown in the current investigation. A large number of studies is not justified in any CFD investigation performed by Devahastin and Mujumdar [9]. Also, the CFD needs to be verified systematically for laminar and turbulence flow separately and independently [10]. The unnecessarily fined mesh could lead a wrong conclusion.

The very wrong approach to validate CFD results without satisfying the verification requirement. This is not a crude practice. It may be the case that the researchers are using more or less mesh than it requires. For example,

Wilson and Imber [11] studied a computational model of a rectangular jet ($Re_j = \frac{d_0 u_0 \rho_l}{\mu_l} = 1.49 \times 10^5$) with aspect

ratio 10. It would be interesting to investigate the effect of doubling the mesh of Wilson and Imber [11]. This investigation could be helpful for more applied pipeline oil flow under the sea [12] or under the ground [13].

The approach used by Devahastin and Mujumdar [9] would force the researchers to cause unnecessary wastes of computing resources (by running longer time for low Reynolds number). This approach is not followed here. Rather, each case has been checked for grid independence.

Here in the research: next section defines the computational physics, followed by experimental setup and computational models, results are presented with verification and validation. The conclusions are added next. Presenting the grid independence behavior offers more satisfaction [14]. The mixing zone analysis needs the outcome of a submerged jet [15]. When the free surface is involved like in an in an impinging jet, the flow becomes more complex [16]. The heated flow the validation process is very complicated as the experimental process has limitations as in these cases [17, 18]. For a bigger domain [19], the experimental data is not easy to collect. For simplicity, the oscillation or fluctuation [20] is not considered which did introduce error. All kind of absorption [21, 22] of air is neglected for simplicity.

2 COMPUTATIONAL PHYSICS

An axisymmetric geometry is considered which represent the cylindrical receiving bath of 500 mm long (H_c) with a diameter (D_c) of 90 mm (Figure 1). At the center of the cylinder from the top roof the nozzle comes vertically down and the tip of the nozzle is 355 mm above the base or 145 mm below the top of the cylinder wall, only 145 mm is inside the receiving cylindrical bath (the rest 55 mm is not shown). Concerning Figure 1, outlet pipe the jet is located $0 \leq r \leq 6$ and cylinder is located at $-145 \leq X \leq 355$ mm and $0 \leq r \leq 45$ mm, and inlet jet is defined as $0 \leq r \leq 4.8$ mm for the inlet jet, $355 \text{ mm} \leq X \leq 555$ mm and mm for the outlet pipe in the bottom.

An inlet boundary condition was set at nozzle inlet, and this is 200 mm of length. An outlet pipe BC was used at the domain outlet. The tip of the exit pipe is 200 mm below the base. The mass flow rate of the inlet a outlet are kept same so there is no rise of liquid air surface level while running the experimental or computation test. It was easier to set a no accumulation zone; however, experimentally its was nearly hard. The circular outlet pipe (Figure 1) will not be shown in the rest of the figures of this paper.

3 EXPERIMENTAL SETUP

For the submerged liquid jet, Laser Doppler Velocimetry (LDV) data were taken to validate the computational results of the primary flow. A schematic diagram of the experimental arrangement is shown in Figure 2. The major equipment consists is a cylindrical receiving bath ($D_c = 90$ mm, $H_c = 500$ mm), a nozzle ($d_0 = 9.6$ mm), a reservoir tank, a pump to recirculate the water. The size of the nozzle, the receiving cylinder, and the outlet are identical to those in computational models. The level of water in the cylinder is kept constant by controlling the flow.

For a 100 mm nozzle submergence depth, there was no significant oscillation in the free liquid surface in the cylindrical bath. So for a 100 mm of h , the free surface was considered as a wall (with zero shear stress) in the computational models. In the experiments, even though efforts were made to keep a 'no accumulation' of water in the cylindrical bath, in reality, it was not strictly possible. This minor variation was unfavorable. The liquid in the bath was stationary before switching on liquid jet both for the computational techniques and for experimentations.

4 COMPUTATIONAL MODELS

Continuity, momentum equations along with $k - \varepsilon$ Realizable [23], *RSM* [24, 25], and *SST* [26] turbulence models were used to solve the fluid flow by an SJ. The detail verification of grid refinement is presented in the results section. The level of convergence was of the order of 10^{-6} . Consistency higher order discretizations and pressure-velocity coupling [27] were used in all cases studied. The computational modeling parameters were determined after verification [28] and validations [29].

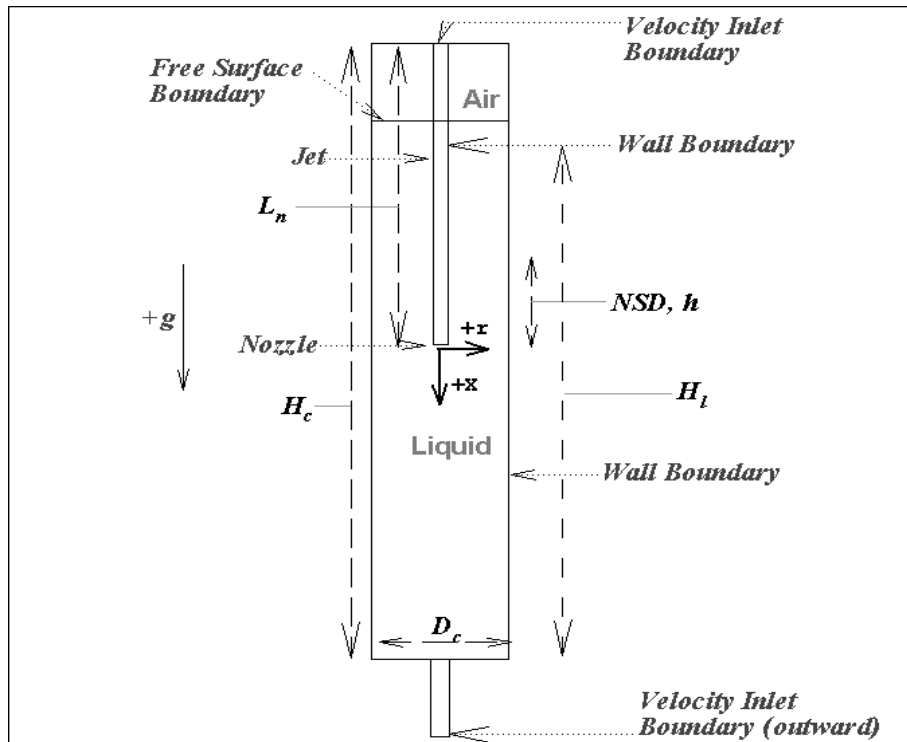


Figure 1: A schematic diagram of the computational domain of the submerged liquid jet apparatus with the boundary conditions [$d_{in} = 9.6$ mm, $D_c = 90$ mm, $H_l = 455$ mm, $H_c = 500$ mm, $h = 100$ mm, outlet nozzle, $d_{out} = 12$ mm].

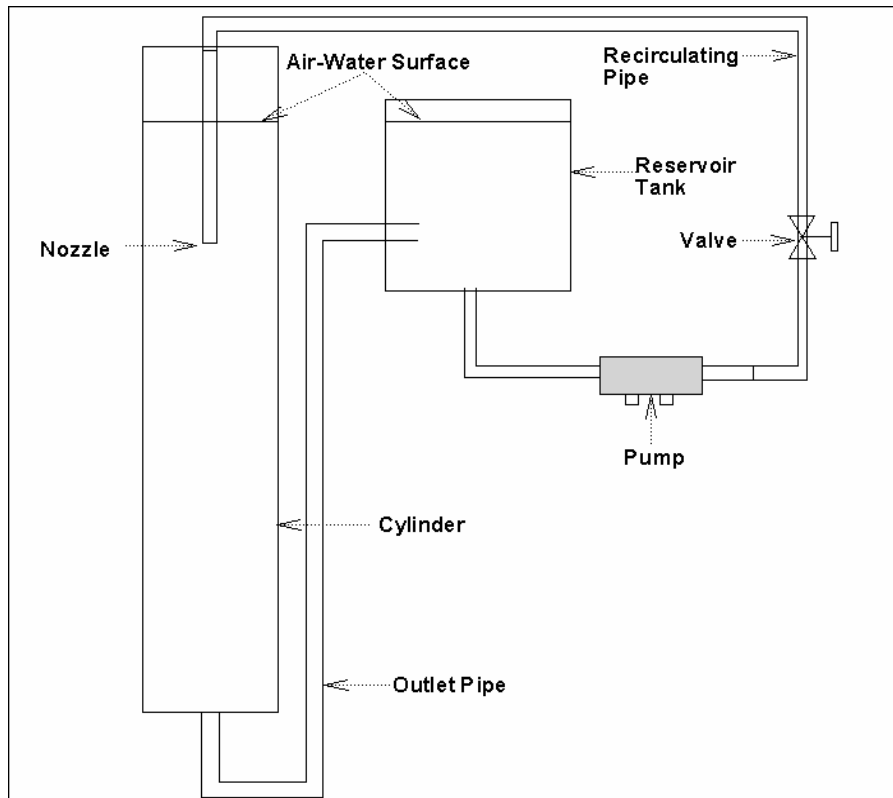


Figure 2: Experimental Set Up of the Submerged Liquid Jet

5 RESULTS AND DISCUSSIONS

Using refinement as presented in this section ensures the less grid dependence solution. All the turbulence parameters (turbulent kinetic energy k , turbulent intensity ($\sqrt{2k/3}/U$), turbulent dissipation rate, ε) and primary flow parameters (velocity) are examined for this purpose as the refinement performed, even though a few are presented here.

Figure 3 presents a typical case where the center line velocity magnitude (m/s) (left-hand side) and center line turbulence kinetic energy (k) (right-hand side) have been plotted against nondimensional distance from the nozzle (X/D_c) for four quadrilateral meshes (mesh0=32,550, mesh1=40,100, mesh2=43,875, mesh3=54,000). In both these cases, it is clearly shown that on mesh3, the solution parameters have reached their asymptotic levels. Even mesh2 and mesh1 are fine enough to predict the velocity and turbulent kinetic energy. The mesh density is higher near the nozzle region compared to the rest of the domain to capture the sharp gradient of solution parameters. Figure 3 (left) shows that at about 0.75-1.25 of X/D_c , the center line velocity is most sensitive to the choice of grid size. It is repeatedly found in many CFD papers that the authors check only one parameter (especially velocity components) as the refinement continues; however, Figure 3 (right-hand side) show that the turbulent kinetic energy does not behave the same way as the velocity magnitude (left-hand side of Figure 3). The peak kinetic turbulent energy is at $1.0 X/D_c$ (right-hand side of Figure 3) and k is very sensitive in the (0.60-1.10) X/D_c region. Sensitivity of turbulence intensity (left hand side, Figure 4), turbulent dissipation rate (right hand side, Figure 5), rate of change of axial velocity in the axial direction (left hand side, Figure 5) and strain rate (right hand side, Figure 5) with the four meshes considered are presented.

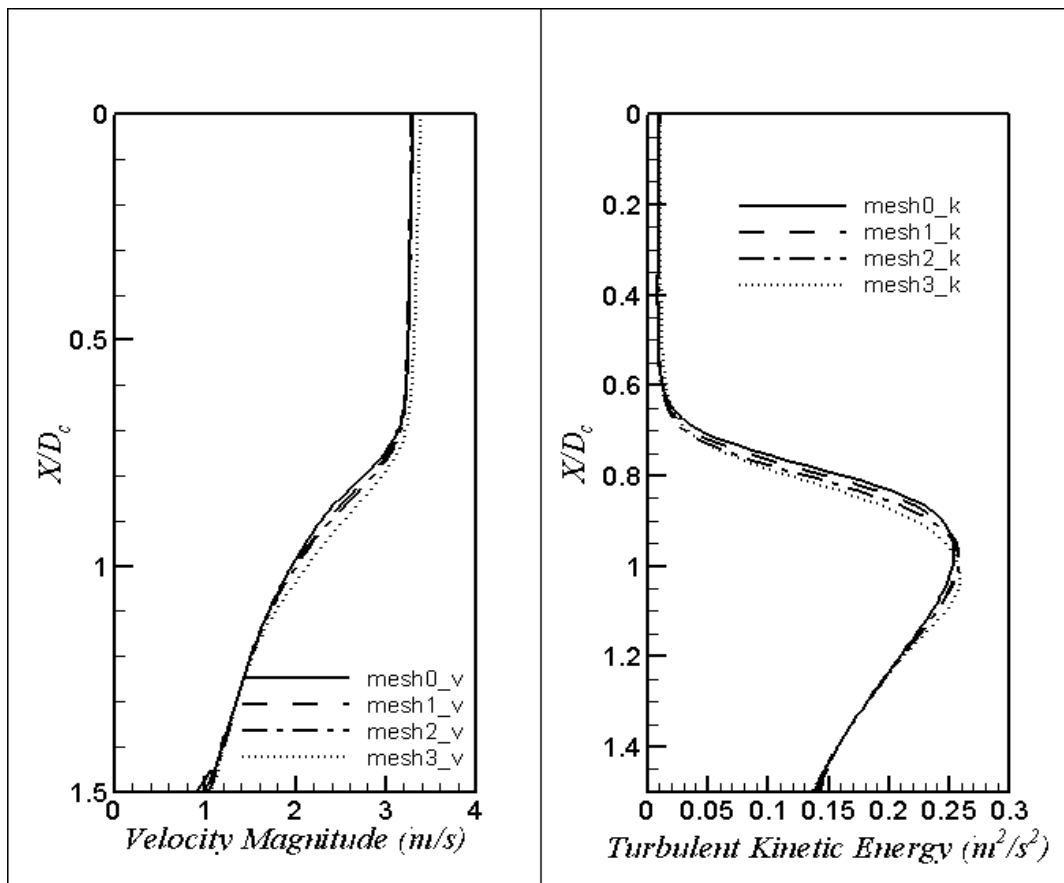


Figure 3: Center line velocity magnitude (m/s) and turbulent kinetic energy for four different meshes [$V_q = 12$ liter/min, symbols are shown in Figure 1].

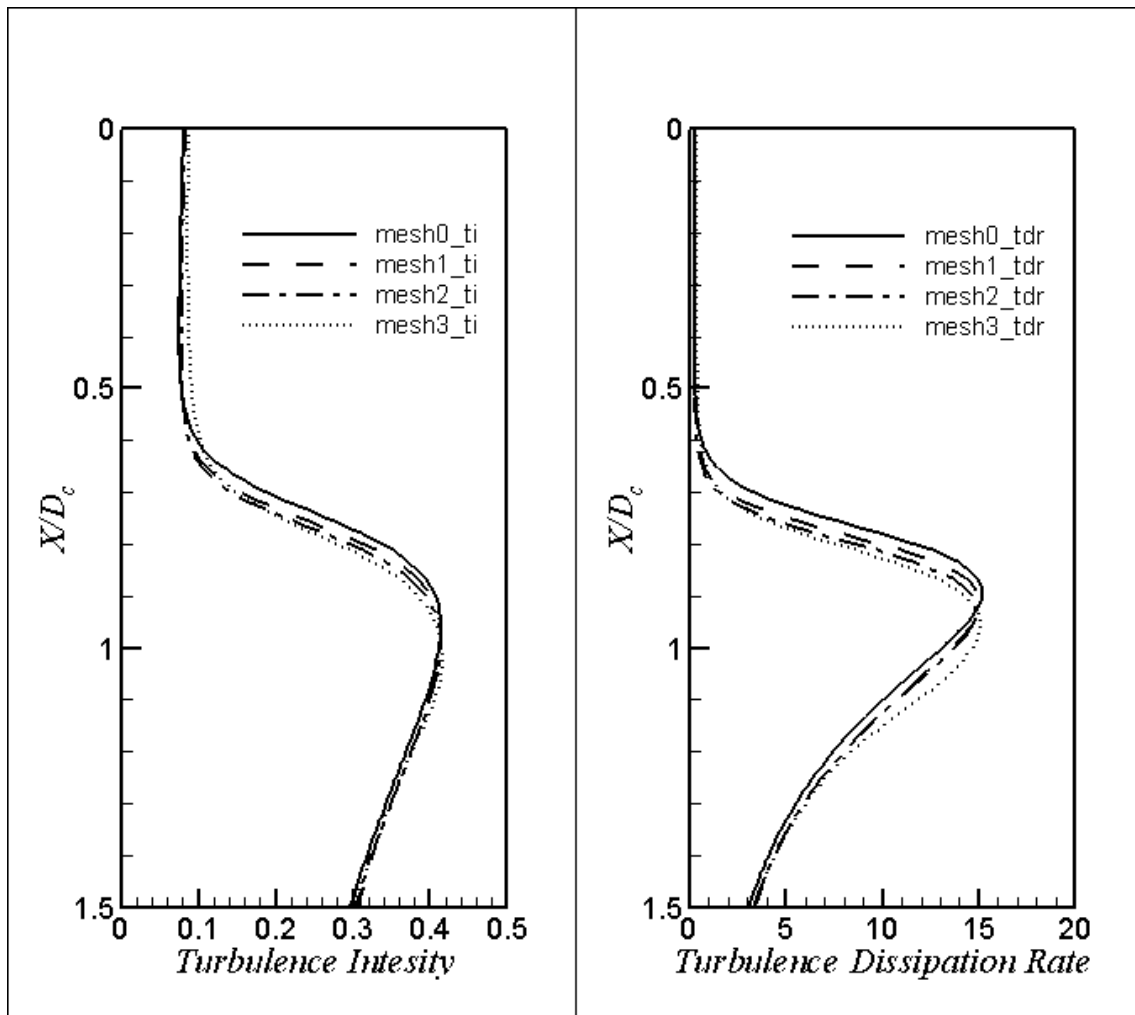


Figure 4: Left: center line turbulent intensity, right turbulent dissipation rate for three different meshes [$V_q=12$ liter/min].

The turbulent intensity (left-hand side of Figure 4) is more sensitive at the inlet ($X/D_c=0.50-1.0$), whereas the turbulent dissipation rate (Figure 4, right) has a similar pattern to the turbulent kinetic energy (Figure 3, right). It should be noted that the inlet liquid jet is 40 times in length the nozzle radius for all the results presented. Hence when the liquid jet exits to the cylindrical bath ($X/D_c=0.0$), the flow is fully developed. At the inlet, the turbulent intensity ($\sqrt{2k/3}/U_0 * 100$) was set 10%, and after flowing 200 mm (L_n of Figure 1), at the nozzle exit ($X/D_c=0.0$) to the receiving bath, the developed turbulent intensity is $\sim 11\%$ as found in Figure 4 (left-hand side). The rate of change of solution parameters is more sensitive to grid size as shown Figure 5. The left of Figure 5 shows that rate of change of axial velocity along an axial direction, which suggests that dU/dX is more sensitive than the corresponding velocity (left-hand side of Figure 3). However, solutions on mesh3 have reached the asymptotic level (Figure 3, Figure 4 and Figure 5). The center line strain rate (right of Figure 5) is even more sensitive on mesh size, however, again found that the strain rate of the centre line on mesh3 (right-hand side of Figure 5) is less dependent on the mesh. In fact, solution on mesh2 is fine enough to predict the center line solution parameters.

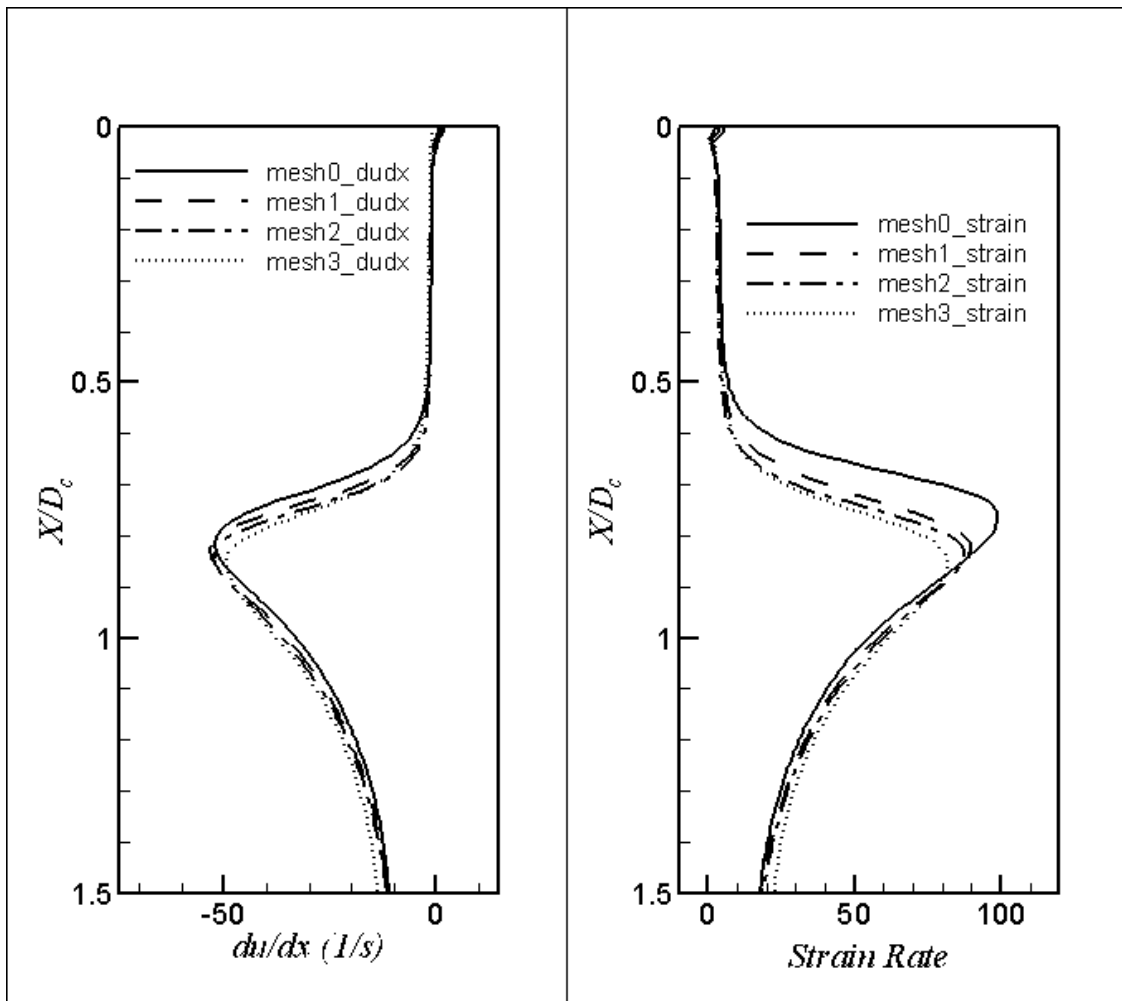


Figure 5: Left: center line axial velocity gradient (dU/dX), right: center line strain rate for three different meshes [$V_q = 12$ liter/min].

The verification of the dependence of solution parameters on grid size in the center line does not guarantee that the solution is independent of the grid in the rest of the domain. The variations of two solution parameters, e.g., axial velocity and turbulent kinetic energy at 100 mm ($X/D_c = 1.11$) down from the nozzle along the non-dimensional radial direction (r/R_c) are shown in Figure 6, left and right, respectively. Figure 6 shows that up to $r/R_c = 0.18$, both the axial velocity and turbulent kinetic energy are sensitive to grid size. However, the mesh3 solution does not significantly differ from the solution on mesh2. Where the gradient of solution parameters is higher, the solution parameters (velocity, turbulent kinetic energy, turbulent intensity, turbulent dissipation rate, etc) are more sensitive to mesh size compared to the rest of the domain. In all the sections presented next, only mesh2 is used which is less dependent on mesh size as shown in general. The results in Figure 6 also indicates that the local refinement is necessary to capture the physics in the core of the jet as concluded by others [30] as well. Figure 7 presents the center line mean velocity magnitude (left-hand side) and center line turbulent kinetic energy (k) (right-hand side) as a function of dimensionless distance from the nozzle exit (X/D_c) for $k-\varepsilon$ Realizable (referred as KERZ), RSM and SST turbulence models. The black squares (Figure 7) show the experimental data.

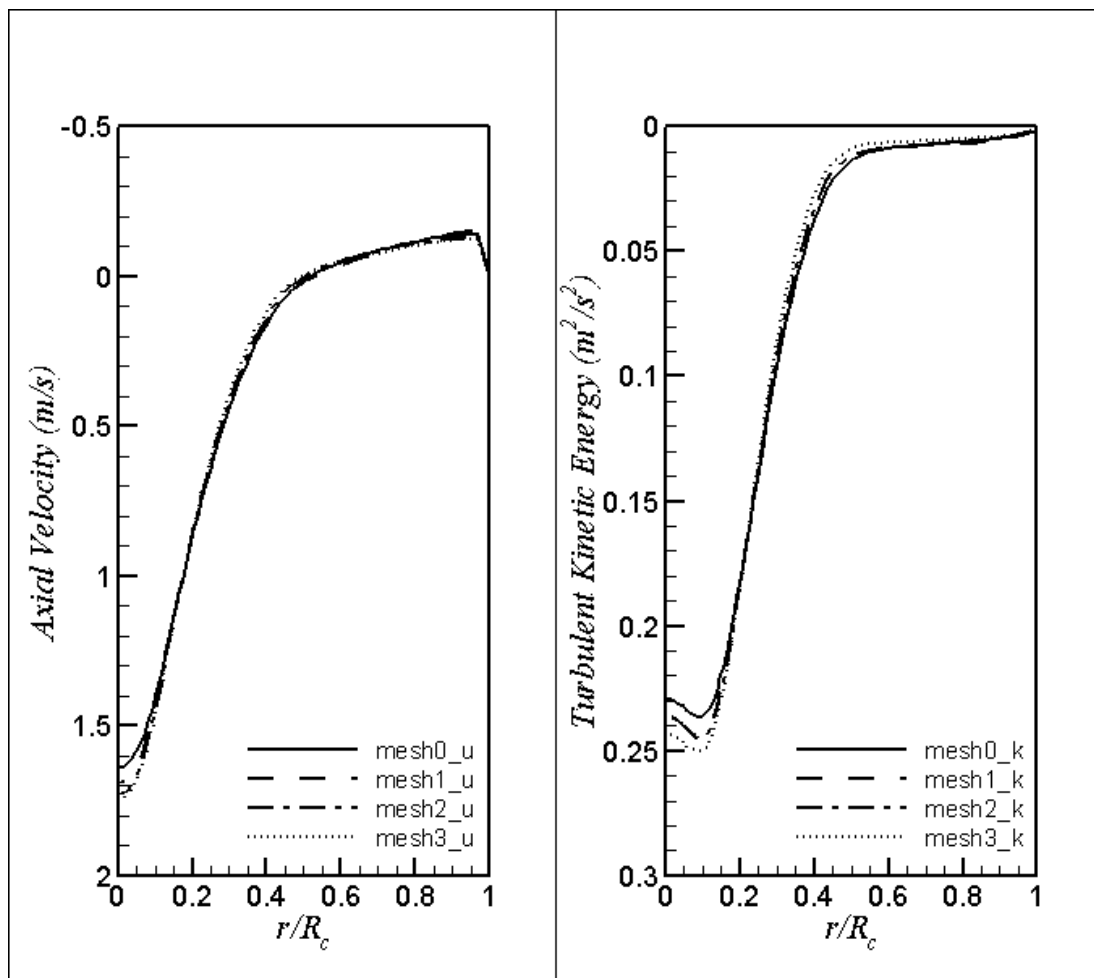


Figure 6: Radial variation turbulent kinetic energy (left) and turbulent intensity (right) at 100 mm below the nozzle for three different meshes [$V_q = 12$ liter/min].

The experimental velocity magnitude (left of Figure 7) is calculated by the sqrt of 3 velocity components $\sqrt{(v_x^2 + v_y^2 + v_z^2)}$. Figure 7 (left) shows in terms of velocity magnitude production, both $k-\varepsilon$ Realizable and RSM are of same accurate for $X/D_c = 1.0-3.0$, however, for $X/D_c < 1.0$, RSM is better. SST is the better in predicting the center line velocity. Within $X/D_c = 0.8-1.0$ and $X/D_c = 2.0-3.0$, a higher discrepancy is noticed. The former discrepancy is probably because SST is not very accurate in predicting sharp gradient in velocity. The second discrepancy is due to the bottom exit. The solution is not steady near the exit of the domain.

Figure 7 (right) shows that in the range of $X/D_c = 0-1.0$, $k-\varepsilon$ Realizable and SST fail to predict the turbulent kinetic energy, whereas the RSM can predict the k better. The experimental turbulent kinetic energy is calculated as $\frac{1}{2}(\sigma_x^2 + \sigma_y^2 + \sigma_z^2)$, where σ_i is the root mean square velocity components. Next, to the nozzle exit, the higher gradient of velocity (left of Figure 6) exists, which may result in high turbulence as can be seen from Figure 7 (right). From Figure 5, the mean axial velocity is same up to $0.75 X/D_c$, after this, there is a sharp decrease in axial velocity resulting in higher turbulence kinetic energy. It is ongoing on how to calculate the experimental turbulent kinetic energy. The non-isentropic experimental σ_y compared to σ_x is carefully noticed.

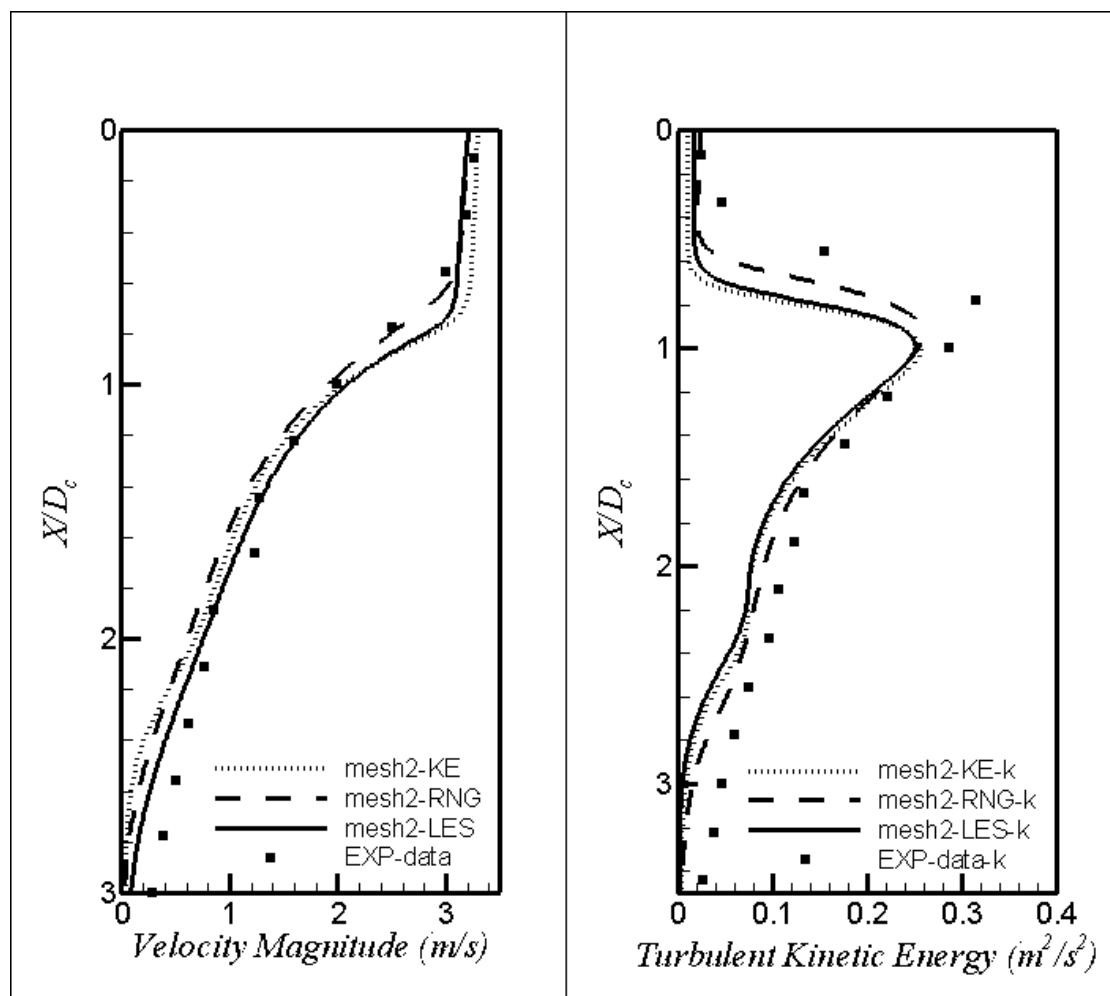


Figure 7: Computational (solid lines) and experimental (black squares) centre line velocity magnitude (m/s) and turbulence kinetic energy (k) [$V_q = 12$ litre/min].

6 CONCLUSIONS

The step-by-step verification and validation process will remind the researchers how important it is to follow the steps of these processes. Forced to consider to an axisymmetric flow, computationally it was cheap, which will serve the purpose of many industrial applications. It was found the *SST* model predicts the flow field more closely to the experimental data compared to $k - \varepsilon$ Realizable and *RSM*.

The models developed here could easily be broadened for liquid jets with a definite swirling flow. However, in most cases, the swirling nature is challenging to report from the experimental data. The experimental data could be used to test any CFD code, as shown here.

REFERENCES

1. Nawaf H. Saeid NH, Ali MHBHM. Effect of the metallic foam heat sink shape on the mixed convection jet impingement cooling of a horizontal surface (in press). *Journal of Porous Media* 2017.
2. Oosterhuis JP, Timmer MAG, Bühler S, Van Der Meer TH, Wilcox D. On the performance and flow characteristics of jet pumps with multiple orifices. *Journal of the Acoustical Society of America* 2016;139:2732-40.
3. Strykowski PJ, Niccum DL. The influence of velocity and density ratio on the dynamics of spatially developing mixing layers. *Physics of Fluids A: Fluid Dynamics* 1992;4:770-81.
4. Yang Y, Crowe CT, Chung JN, Troutt TR. Experiments on particle dispersion in a plane wake. *International Journal of Multiphase Flow* 2000;26:1583-607.

5. Zhong W, Yu A, Liu X, Tong Z, Zhang H. DEM/CFD-DEM Modelling of Non-spherical Particulate Systems: Theoretical Developments and Applications. *Powder Technology* 2016;302:108-52.
6. Azpiroz JE, Hendrix MHW, Breugem WP, Henkes RAWM, editors. CFD modelling of bypass pigs with a deflector disk. BHR Group - 17th International Conference on Multiphase Technology 2015; 2015.
7. Zhalehrajabi E, Rahmanian N, Hasan N. Effects of mesh grid and turbulence models on heat transfer coefficient in a convergent–divergent nozzle. *Asia-Pacific Journal of Chemical Engineering* 2014;9:265–71.
8. Bayly AE, Rielly CD, Evans GM, Hazell M, editors. The Rate of Expansion of A Confined, Submerged Jet. 20th Australasian Chemical Engineering Conference, Canberra; 1992.
9. Devahastin S, Mujumdar AS. A numerical study of flow and mixing characteristics of laminar confined impinging streams. *Chemical Engineering Journal (Amsterdam, Netherlands)* 2002;85:215-23.
10. Hosseinalipour SM, Mujumdar AS. Flow and thermal characteristics of steady two dimensional confined laminar opposing jets. Part I. Equal jets. *Int Commun Heat Mass* 1997;24:27-38.
11. Wilson WM, Imber RD, editors. CFD Analysis of Compact, High Aspect Ratio Ejectors. *Proceedings of ASME FEDSM*; 2001.
12. Koh Junyi NH. Review of the Factors that Influence the Condition of Wax Deposition in Subsea Pipelines. *International Journal of Materials and Manufacture* 2018;3;1:1-8.
13. Ishak MA, Islam MA, Shalaby MR, Hasan N. The Application of Seismic Attributes and Wheeler Transformations for the Geomorphological Interpretation of Stratigraphic Surfaces: A Case Study of the F3 Block, Dutch Offshore Sector, North Sea. *Geosciences* 2018;8:79.
14. Zhalehrajabi E, Rahmanian N, Hasan N. Effects of mesh grid and turbulence models on heat transfer coefficient in a convergent–divergent nozzle. *Asia-Pacific Journal of Chemical Engineering* 2014;9:265-71.
15. Hasan N. CFD analysis of the mixing zone for a submerged jet system. *ASME Fluids Engineering* 2001.
16. Khan MN, Fletcher C, Evans G, He Q. CFD Modeling of Free Surface and Entrainment of Buoyant Particles From Free Surface for Submerged Jet Systems. *ASME-PUBLICATIONS-HTD* 2001;369:115-20.
17. Nurul Hasan PW, Geoffrey Brooks., Nagle M, editors. Design of supersonic nozzles for ultra-rapid quenching of metallic Vapours. *TMS Annual Meeting*; 2006.
18. Hasan N. CFD modelling of heat transfer in supersonic nozzles for magnesium production. *TMS Journal* 2007.
19. Naser J, Alam F, Hasan N, editors. Evaluation of a proposed dust ventilation/collection system in an underground mine crushing plant. 16th Australasian Fluid Mechanics Conference (AFMC); 2007: The University of School of Engineering.
20. Sern WK, Takriff MS, Kartom S, Kamarudin MZMT, Hasan N. Numerical Simulation of Fluid Flow Behaviour On Scale Up Of Oscillatory Baffled Column. *Journal of Engineering Science and Technology* 2012;7:119-30.
21. Harith Rashid NH, M. Iskandar M. Nor. Accurate Modeling of Evaporation and Enthalpy of Vapor Phase in CO₂ Absorption by Amine Based Solution. *Separation Science and Technology* 2014;49:9:1326-34.
22. Rashid H, Hasan N, Nor M, Iskandar M. Temperature Peak Analysis and Its Effect on Absorption Column for CO₂ Capture Process at Different Operating Conditions. *Chemical Product and Process Modeling* 2014.
23. Shih T-H, Liou WW, Shabbir A, Yang Z, Zhu J. A New k-Epsilon eddy viscosity model for high Reynolds number turbulent flows. *Computers and Fluids* 1995;24:227-38.
24. Dupont V, Pourkashanian M, Williams A, Woolley R. The reduction of nitrogen oxide (NO_x) formation in natural gas burner flames. *Fuel* 1993;72:497-503.
25. Henkes RAWM, Hoogendoorn CJ. Scaling of the turbulent natural convection flow in a heated square cavity. *Journal of Heat Transfer: Transactions of the ASME* 1994;116:400-8.
26. Menter FR. Two-Equation Eddy-Viscosity Turbulence Models for Engineering Applications. *AIAA Journal* 1994;32:1598–605.
27. Ferziger JL, Peric M. *Computational Methods for Fluid Dynamics*: Springer-Verlag, Heidelberg.; 1996.
28. Roache PJ. *Verification and Validation in Computational Science and Engineering*. first ed: Albuquerque, N.M.: Hermosa publishers; 1998.
29. Hasan N. *CFD Studies on Fluid-Particle Interactions on Free Surface Flows*. The University of New South Wales, 2003.
30. Gardin P, Brunet M, Domgin JF, Pericleous K. An experimental and numerical CFD study of turbulence in a tundish container. *Applied Mathematical Modelling* 2002;26:323-36.